Journal of Applied Polymer Science

Mechanical performance and flame retardancy of polypropylene composites containing zeolite and multiwalled carbon nanotubes

Qing Zhao,[1] Yanhong Hu,[2] Xingyi Wang[1]

[1]Laboratory for Advanced Materials, Research Institute of Industrial Catalysis, East China University of Science and Technology, Shanghai 200237, People's Republic of China

[2]Key Laboratory for Specially Functional Polymers and Related Technology of the Ministry of Education, School of Materials Science and Engineering, East China University of Science and Technology, Shanghai200237, People's Republic of China

Correspondence to: Y. Hu (E-mail: huyhxy@ecust.edu.cn) and X. Wang (E-mail: wangxy@ecust.edu.cn)

ABSTRACT: Intumescent-flame-retarded polypropylene (PP-IFR) composites were prepared by the incorporation of methyl hydrogen siloxane treated ammonium polyphosphate and dipentaerythritol in a twin-screw extruder. The effects of zeolite (Z), multiwalled carbon nanotubes (CNTs), and maleic anhydride grafted polypropylene on the flame retardancy, mechanical properties, and thermal stability of PP-IFR were investigated. The addition of Z and CNT promoted the flame retardancy of PP-IFR, and the highest limited oxygen index was 35.6%, obtained on PP-M-IFR-2–Z, for which the heat-release rate, total heat release, and smoke production rate based on cone calorimetry analyses decreased by 45.0, 51.0, and 66.3%, respectively, in comparison with those values of the PP-IFR composites. Additionally, scanning electron microscopy analyses showed that there was a good interface interaction between the polypropylene matrix and additives. The flexural, tensile, and impact strengths of the PP-IFR composites were improved significantly with the incorporation of CNT. © 2015 Wiley Periodicals, Inc. J. Appl. Polym. Sci. **2016**, *133*, 42875.

KEYWORDS: flame retardance; mechanical properties; thermal properties

Received 24 January 2015; accepted 23 August 2015
DOI: 10.1002/app.42875

INTRODUCTION

Polypropylene (PP) is an important semicrystalline thermoplastic that is widely used in many fields, including automobiles, building materials, transport, and electrical engineering, because of its excellent processability, outstanding chemical resistance, good mechanical properties, and low cost.[1–3] However, its high flammability [17% limited oxygen index (LOI)] has limited applications in some fields where flame retardancy is required.[4] Flame retardancy can be promoted greatly by the addition of flame-retardant additives.[5] Intumescent flame retardants (IFRs) have been arousing more and more attention in recent years because some of their merits, including very low toxic gas, small smoke production during burning, and antidripping properties, compared with traditional halogen-containing flame retardants.[6–9]

Generally, IFRs are typical condensed-phase flame retardants that are composed of acid, carbon, and gas sources[10] and work through the formation of an expansion porous carbon layer during thermal decomposition. This carbon layer can slow down the transfers of both heat and oxygen to the burning area and prevent further degradation of the virgin polymer and the volatilization of combustible gas.[11] In the application of IFRs in polymers, however, there are many questions to be solved, including the poor compatibility between polar IFRs and nonpolar polymers, low efficiency,[12,13] migration of IFRs to the polymer surface, and moisture absorption.[14] In recent years, many studies have been done to change this situation. As reported, synergistic agents, such as metallic oxide[15,16] and zeolites (Zs),[17,18] can effectively improve the flame retardancy. On the other hand, the compatibility between the IFR and polymer matrix was improved by the addition of polymeric compatibilizers, such as maleic anhydride grafted polypropylene (MAP).[19–21] Carbon nanotubes (CNTs) have attracted considerable attention because of their extraordinary mechanical properties (e.g., high strength and unique flexibility) and, thus, have often been used as an ideal reinforcing material in composites.[22] Furthermore, CNTs act as a carbon source, forming a heat shield for composites through the *in situ* formation of a protective layer with a continuous network structure[23] to promote the flame retardancy of the polymer composites. In this study, intumescent flame-retarded polypropylene (PP-IFR) composites were prepared by the incorporation of methyl hydrogen siloxane treated ammonium polyphosphate (APP-s) and

Table I. Compositions and Corresponding LOIs of the PP-IFR Composites

Sample	PP (wt %)	APP-s (wt %)	DPER (wt %)	APP-s/DPER (wt %)	LOI (%)
PP	100	0	0	—	17.0
PP-IFR-1-1	75.0	12.5	12.5	1:1	31.9
PP-IFR-2-1	75.0	17.0	8.5	2:1	32.5
PP-IFR-2.5-1	75.0	18.0	7.0	2.5:1	29.4
PP-IFR-3-1	75.0	19.0	6.0	3:1	30.1
PP-IFR-4-1	75.0	20.0	5.0	4:1	28.2

dipentaerythritol (DPER) in a twin-screw extruder. The effects of Z, multiwalled CNTs, and MAP on the combustibility, thermal stability, and mechanical properties of PP-IFR were investigated.

EXPERIMENTAL

Materials

The commercial homopolymer PP, with a melt flow rate index of 2.4 g/10 min (230°C/2.16 kg; Yangzi Petroleum Chemical Co.); untreated ammonium polyphosphate (APP-r; crystalline from II, $n > 1000$; Shanghai Xunshen Halogen-Free Flame Retardant Co., Ltd.); DPER (Jiangsu Ruiyang Chemical Co., Ltd.); MAP, with a grafting rate of 0.8–1.0% and a melt flow index (190°C/2.16 kg) of 40–60 g/10 min (Shenyang Ketong plastics Co., Ltd.); methyl hydrogen siloxane (MHS; KF-99, hydrogen content = 5%, Xinyue Chemical Plant, Japan); 4A Z (Supeng Chemical Co.); and multiwalled CNTs (Chengdu Institute of Organic Chemistry, Chinese Academy of Sciences). The average sizes of APP-r, DEPR, and Z particles were below 10 μm; these were dried in an oven for 12 h at 100°C before use. The other chemicals were used as-received without any further treatment.

Sample Preparation

Microencapsulated APP-r Preparation. 90 g APP-r, 0.9 g MHS, and 180 mL toluene were loaded into a 250-mL, three-necked flask with a stirrer and a reflux condenser; this mixture was then injected and heated to 130°C with reflux for 5 h. After that, the mixture was cooled down to room temperature, filtered, washed with acetone, then dried at 110°C in an oven for 12 h, and finally, ground and bagged for later use. The APP treated with MHS was noted as APP-s. MHS contained active hydrogen species, which may interacte with oxygen species through hydrogen bonding. Because no Si or C on the APP-s sample was detected with EDS limitation, the MHS was expected to be very low.

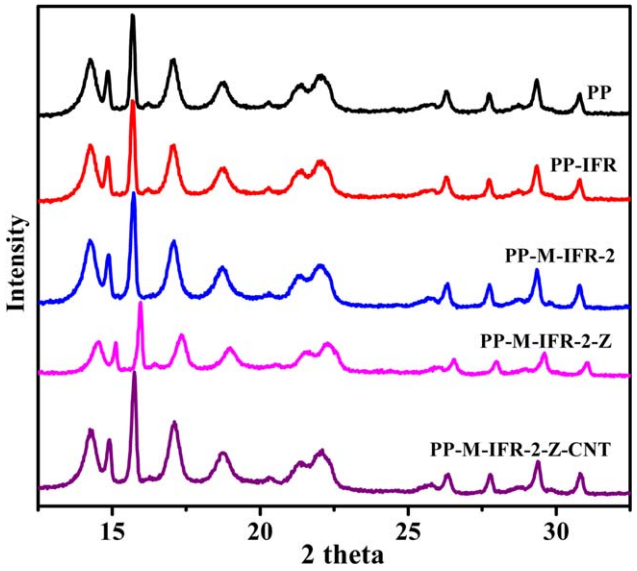

Figure 2. XRD patterns of the PP-IFR composites. [Color figure can be viewed in the online issue, which is available at wileyonlinelibrary.com.]

PP-IFR Preparation. All of the composites (Table I) were prepared in a twin-screw extruder with a roller rotating speed of 60 rpm; the barrel temperature was set at 160°C. First, PP was allowed to melt in the mixer into which the dried additives were added. The ingredients were mixed for 10 min. The mixed material obtained from the mill mold shaping was cut into a corresponding size for testing.

Characterization

Solubility in Water. The solubilities of APP-r and APP-s in water were tested at a given temperature for 1 h and at 30°C for various durations, respectively. 5 g APP-r or 5 g APP-s was put into 50 g distilled water and then stirred for different durations. The filtrate was obtained through filtration, evaporated,

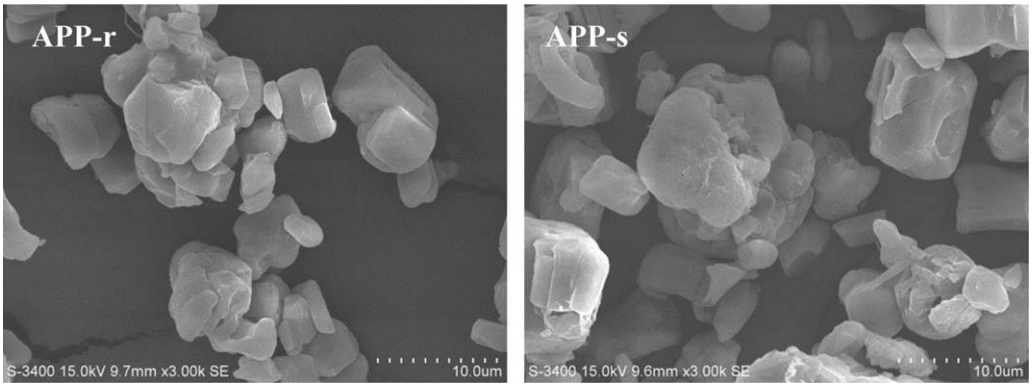

Figure 1. SEM micrographs of the surface morphology of APP-r and APP-s.

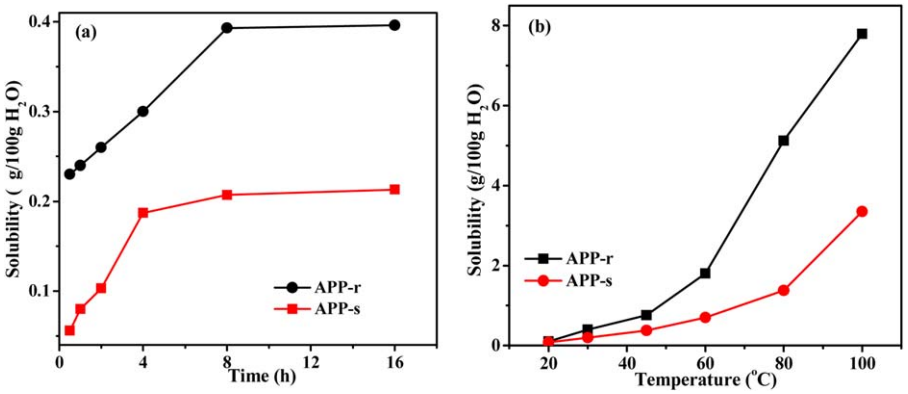

Figure 3. Solubility of APP-s (a) at 30°C for different time durations and (b) at different temperatures for 1 h. [Color figure can be viewed in the online issue, which is available at wileyonlinelibrary.com.]

and finally dried at 120°C until the liquid evaporated completely.

Water Absorption Rate of PP-IFR. The specimens of the PP-IFR-r or PP-IFR-s composites (with a weight noted as W_a) was put in water at different temperatures and kept for 24 h (with a weight noted as W_b). The water absorption rate of the specimens was expressed as follows:

$$\text{Water absorption rate} = (W_b - W_a)/W_a \times 100\%$$

LOI. LOI was measured by a JF-3 oxygen index instrument supplied by Shanghai Cany Precision Instrument Co., Ltd., according to the procedure described in ISO 4589-2, with specimen dimensions of 120 × 6.5 × 3 mm^3.

UL-94 Testing. Vertical burning tests were carried out on a CFZ-2 instrument according to UL-94 test standard with specimen dimensions of 130 × 13 × 3 mm^3.

X-ray Diffraction (XRD) Measurements. XRD measurements were taken on a Rigaku Dmax-3C diffractometer with Cu Kα radiation (40 kV, 30 mA, $\lambda = 0.15408$ nm).

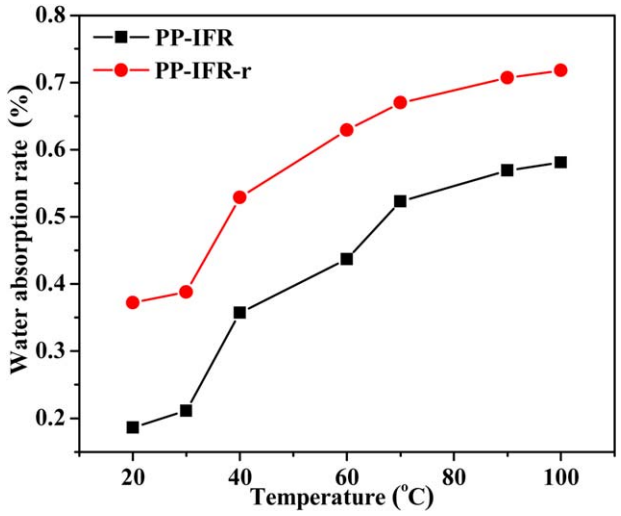

Figure 4. Water absorption rates of PP-IFR-r and PP-IFR at different temperatures after immersion in water for 24 h. [Color figure can be viewed in the online issue, which is available at wileyonlinelibrary.com.]

Mechanical Property Test. The tests for tensile strength and flexural strength were performed on an electronic universal testing machine (CMT5205, Shenzhen Sunthink Science and Technology Development Co., Ltd.) according to ASTM D 638 and ASTM D 790 with crosshead speeds of 5 and 2 mm/min, respectively. The notched Izod impact strength was measured on an Izod impact strength tester at 23 ± 1°C according to ASTM D 256 with specimen dimensions of 50 × 0.6 × 4 mm^3. The presented results are the average values of five parallel experiments.

Morphological Analyses. The morphology of the APP-r and APP-s particles and the fracture and char of the PP-IFR composites were observed with a JSM-6360LV scanning electron microscope with a 60-mA electric current at 15 kV. The fracture of the composites was obtained after impact testing. The specimen surface was sputter-coated by a layer of gold with vacuum evaporation under an argon gas atmosphere before the corresponding images were taken.

Oxygen Consumption Calorimetry. Cone calorimetry tests were performed according to ASTM 1356-90. Each specimen, with dimensions of 100 × 100 × 3 mm^3, was wrapped in aluminum foil and exposed horizontally to an external heat flux of 50 kW/m^2.

Thermogravimetric Analysis (TG). The thermal stabilities of the PP-IFR composites were studied on a TA-2050 thermogravimetric analyzer (TA Instruments) at a heating rate of 10°C/min with a nitrogen flow rate of 100 mL/min. The sample mass was 5–10 mg, and the TG curve was recorded in the heating course from room temperature to 700°C and used to determine the percentage weight loss. The TG results are presented as the temperatures at 5% weight loss ($T_{5\%}$), 10% weight loss ($T_{10\%}$), and 50% weight loss ($T_{50\%}$), which were usually considered as the initial, onset, and midpoint decomposition temperatures, respectively.

Fourier Transform Infrared (FTIR) Spectra. FTIR spectra of all of the samples were obtained at room temperature on a Nicolet 6700 FTIR spectrophotometer (Thermo Fisher Scientific). The char residues obtained at various temperatures were studied in KBr discs within a wave-number range of 500–4000 cm^{-1}.

Table II. Composites with an APP/DPER Ratio of 2:1

Sample	PP (wt %)	IFR (wt %)[a]	MAP (wt %)	Z (wt %)	CNT (wt %)	LOI (%)
PP	100	—	—	—	—	17.0
PP-MAP	98	—	2.0	—	—	18.0
PP-IFR-r[b]	75	25.0	—	—	—	32.0
PP-IFR[a]	75	25.0	—	—	—	32.5
PP-IFR-Z-r[b]	75	25	—	1.0	—	32.5
PP-M-IFR-1[a]	73	25.0	2.0	—	—	32.8
PP-M-IFR-2	69	25.0	6.0	—	—	33.0
PP-M-IFR-1-Z	68	25.0	6.0	0.5	—	34.5
PP-M-IFR-2-Z[a]	68	25.0	6.0	1.0	—	35.6
PP-M-IFR-1-Z-CNT	68	25.0	6.0	1.0	0.05	35
PP-M-IFR-2-Z-CNT[a]	68	25.0	6.0	1.0	0.1	34.3

[a] APP of IFR was treated with MHS.
[b] APP of IFR was not treated.

RESULTS AND DISCUSSION

Morphology of APP-r and APP-s

As shown in scanning electron microscopy (SEM) photos (Figure 1), some ammonium polyphosphate (APP) particles stacked together with others. The sizes of the APP-r and APP-s particles were less than 10 μm. APP-r presented a smoother surface than APP-s did; this was related to MHS coverage.

XRD

XRD patterns of the PP-IFR composites are shown in Figure 2. For PP, there appeared several peaks at 2θ values of 14.3, 17.1, and 18.6°, ascribed to the reflection from the (110), (040), and (130) lattice planes of α crystals, respectively. The peak appearing at a 2θ value of 15.7° was assigned to the reflection from the (300) plane of β crystals. With the addition of APP-s, DPER, Z, and CNTs, no significant changes in the XRD patterns were observed; this indicated that all of the composites maintained the crystal structure of PP.

Water Resistance of the APP and PP-IFR Composites

The water solubility of APP is shown in Figure 3. At 30°C, the solubilities of APP-r in water after stirring for 30 min and 8 h were 0.23 and 0.40 g/100 g of H_2O, respectively, and after that time, remained constant [Figure 3(a)]. However, the solubility of APP-s decreased significantly and was 0.21 g/100 g of H_2O after 16 h of stirring [Figure 3(a)]. The increase in temperature really promoted the solution of APP-s or APP-r in water, but APP-s solvated much more slowly than APP-r did [Figure 3(b)]. This difference increased with temperature; this indicated that a layer of hydrophobic organic silicon coated APP-r during the treatment with MHS and thus resisted water to some extent. Figure 4 shows that the water absorption rates of the PP-IFR-r and PP-IFR-s composites immersed in water for 24 h were 0.37 and 0.19% at 20°C and 0.72 and 0.58% at 100°C, respectively. This significant improvement in the water resistance was also attributed to the hydrophobicity of MHS covered on APP. Obviously, the MHS layer was not destroyed during PP-IFR preparation.

Table III. UL-94 Data for the PP-IFR Composites

Sample	t_1 (s)	t_2 (s)	$t_1 + t_2$ (s)	Flame dripping	UL-94 rating
PP	—	—	—	Yes	No rating
PP-IFR	1.2	5.7	6.9	No	V-0
PP-M-IFR-2	1.2	5.4	6.6	No	V-0
PP-M-IFR-2-Z	1.0	3.9	4.9	No	V-0
PP-M-IFR-2-Z-CNT	1.1	4.2	5.3	No	V-0

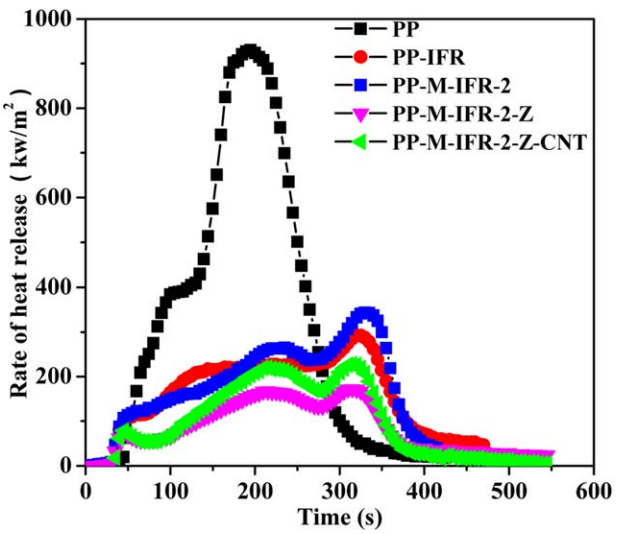

Figure 5. HRRs as a function of time for the PP-IFR composites. [Color figure can be viewed in the online issue, which is available at wileyonlinelibrary.com.]

Table IV. Cone Calorimetry Data for the PP-IFR Composites

Sample	TTI (s)	pk-HRR (Kw/m^2)	THR (MJ/m^2)	Av-EHC (MJ/kg)	Av-SEA (m^2/kg)	pk-SPR (m^2/s)	TSR
PP	30	930	135	33	289	0.113	1783
PP-IFR	19	347	113	42	502	0.046	2474
PP-M-IFR-2	18	380	102	37	517	0.080	2785
PP-M-IFR-2-Z	21	209	50	23	276	0.027	1264
PP-M-IFR-2-Z-CNT	21	226	60	28	281	0.031	1284

LOI and UL-94 Testing

The flame-retardant efficiency depends on the coordination of various functions, wherein the component ratio is an important factor.[24] The effect of the APP-s/DPER ratio on the LOI value of composites was investigated. As shown in Table I, LOI value of the pure PP was only 17%; this indicated that PP was easily flammable. With the addition of APP-s and DPER in an APP-s/DPER ratio range of 1–4, the LOI value increased greatly up to 28.2–32.5%. The PP-IFR-2-1 sample with an APP/DPER ratio of 2 showed the highest LOI value of 32.5%. A further increase in APP-s caused the decrease in the LOI value. As known, APP-s is a type of phosphorus–nitrogen flame retardant containing acid and gas sources. On heating, the acid source catalyzed the dehydration of hydroxyl groups of DPER to form coal (which could prevent oxygen from contacting the composites) and release inflammable gases (which could dilute the oxygen concentration). Therefore, the synergy between APP-s and DPER was a key factor in raising the flame retardancy. In this study, the ratio of APP-s/DPER was set at 2:1. Additionally, the addition of 0.5–1 wt % Z increased new Bronsted acid sites; this further catalyzed the carbonation and thus increased the LOI value to 35.6% (Table II).

The UL-94 data of the PP-IFR composites are given in Table III. The burning times after first ignition (t_1) and second ignition (t_2) and the total combustion time ($t_1 + t_2$) were recorded during UL-94 tests, and the average burning time of the five tests are shown in Table III. For rational comparison, a burning time of 50 s was designated for calculation when nonextinguishment occurred in the test. PP burned out with the occurrence of dripping during burning and thus could not pass any rating. The PP-IFR composites containing 25% IFR passed the V-0 rating (short burning time and no dripping). With the addition of 1% Z, the burning time became much shorter and decreased from 6.9 to 4.9 s; this indicated that Z improved the flame retardancy of the PP-IFR composites.

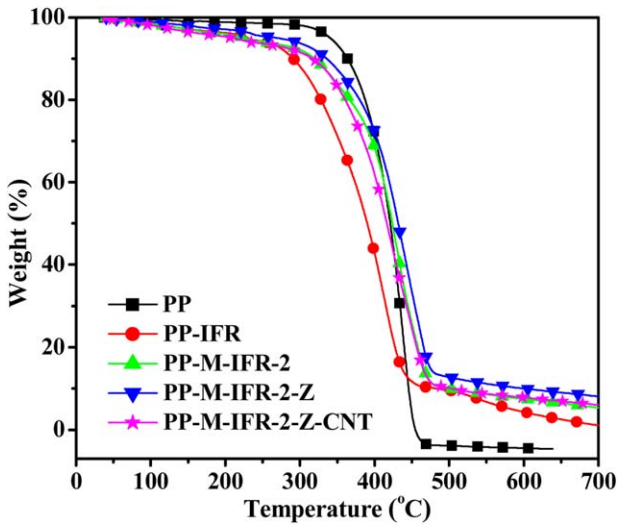

Figure 6. TG curves of the PP-IFR composites. [Color figure can be viewed in the online issue, which is available at wileyonlinelibrary.com.]

Combustion Behavior

Cone calorimetry is one of the most effective bench-scale methods for studying the flammability properties of a material. The heat-release rate (HRR) and total heat release (THR) are the most important parameters in evaluating fire safety.[27] Figure 5 shows that pure PP burns very fast after ignition at a heat flux 50 kW/m^2. A sharp HRR peak appeared at a rate of heat release of 930 kW/m^2, and THR reached 125 kJ/m^2 within 360 s. For PP-IFR, PP-M-IFR-2, PP-M-IFR-2–Z, and PP-M-IFR-2–Z–CNT, the peak HRR values decreased greatly to 347, 380, 209, and 226 kW/m^2, respectively (Table IV). Two or three HRR peaks appeared in these composites because of the collapse of the charred structure; this led to the liberation of trapped volatiles, as reported previously.[28] The THR shown in Table IV followed the order PP-M-IFR-2 < PP-IFR < PP-M-IFR-2–Z–CNT < PP-M-IFR-2–Z; this indicated that under the action of the Bronsted acidic sites of Z, IFR carbonated and retarded the heat release more effectively.

Thermal Stability

Figure 6 shows the TG curves of the PP-IFR composites. In a nitrogen atmosphere, the decomposition of the pure PP started at about 370°C; this became quick with the increase in the temperature, and reached completion at about 454°C (Table V). For all of the PP-IFR composites, the onset decomposition shifted to a low temperature of 120°C because of the evolution of NH_3 and H_2O from APP-s and DPER at a lower temperature.[29] At 450°C, for the pure PP, PP-IFR, and PP-M-IFR-2, the char residues were 3.0, 11.7, and 25.1%, respectively. With the addition of Z, the char residues increased to 32.8%. Here, Z acted as a catalyst and promoted the formation of char during the decomposition of PP-IFR. When the temperature was raised to 700°C, a significant amount of char residues existed for the PP-IFR composites.

Table V. TG Data for the PP-IFR Composites

Sample	Decomposition temperatures (°C)				Residue (wt %)		
	$T_{5\%}$	$T_{10\%}$	$T_{50\%}$	T_{max}	450°C	600°C	700°C
PP	341	363	421	439	3.1	—	—
PP-IFR	231	291	390	414	11.7	4.3	1.1
PP-M-IFR-2	229	319	424	430	25.1	7.5	5.4
PP-M-IFR-2-Z	270	336	432	437	32.8	10.3	7.8
PP-M-IFR-2-Z-CNT	210	317	417	422	24.1	7.8	6.0

SEM Analyses on the Char

To investigate the effects of Z and CNTs on char formation during PP-IFR burning, the morphologies of chars obtained during the heating of the samples at 500°C for 30 min in air were examined by SEM. As shown in Figure 7, the char layers of PP-IFR were composed of islands. With the addition of 1% Z, the islands became larger and planer, and this indicated that the char layer became dense. For PP-M-IFR-2–Z–CNT, the char layer presented a dense, expanded and thick morphology, although some small holes appeared. This was different from PP-IFR and PP-M-IFR-2–Z. As reported, the CNTs acted as a heat shield for the composites through the *in situ* formation of a continuous, network-structured protective carbon layer;[23] this promoted the flame retardancy.

The FTIR spectra of the chars obtained after the treatments of PP-IFR, PP-M-IFR-2, and PP-M-IFR-2–Z in air at 300, 400, and 500°C for 10 min are shown in Figure 8. A strong peak appearing at 3379 cm^{-1} was ascribed to N—H bonds. A peak at 3157 cm^{-1} was ascribed to C—OH or P—OH bonds. Four peaks at 2968, 2919, 2868, and 2838 cm^{-1} were ascribed to C—H bonds. Two peaks at 1017 and 725 cm^{-1} were ascribed to P—O—C bonds, and a peak at 1165 cm^{-1} was ascribed to C—O—C. When the temperature increased, C—OH in DPER dehydrated to form C—O—C bonds before the PP matrix began to degrade. At higher temperature, the remaining species further decomposed into complexes containing stable polyphosphate with P—O—C. The high flame retardancy of PP-IFR was related to the formation of P—O—C. It should be pointed out that during the decomposition of PP-IFR, the incorporation of MAP promoted the degradation of PP-IFR at 400°C, where C—H bands appearing at 2968, 2919, 2868, and 2838 cm^{-1} almost completely disappeared from the FTIR spectra; this was

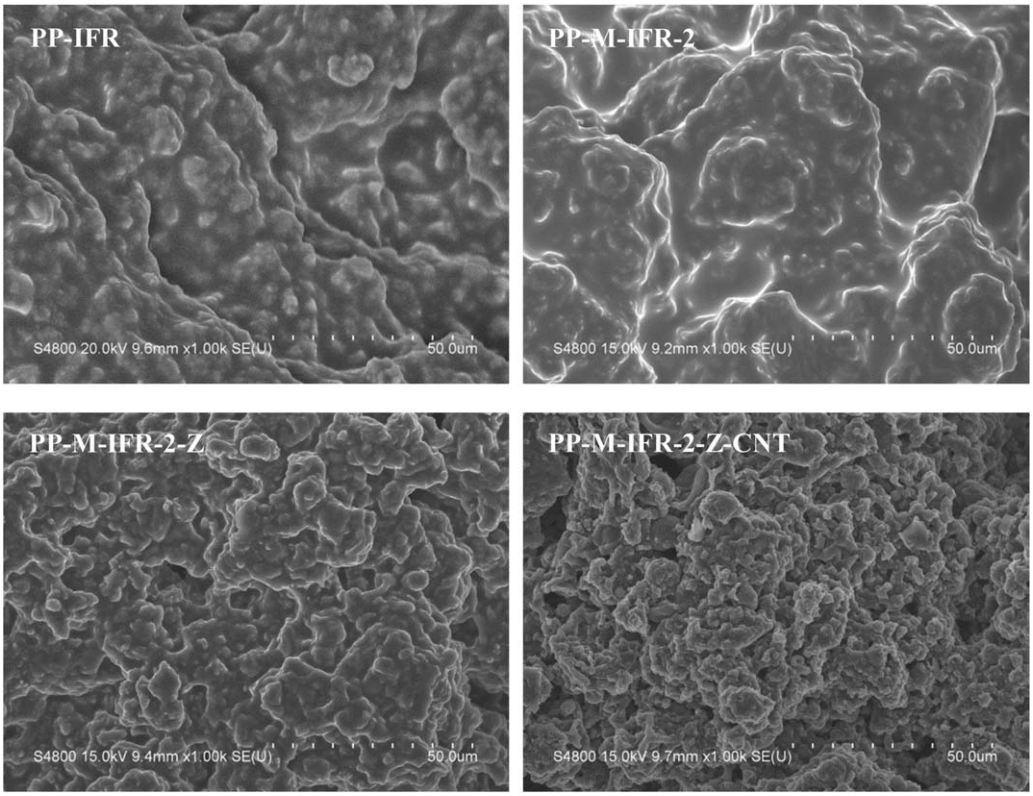

Figure 7. SEM micrographs of the PP-IFR char.

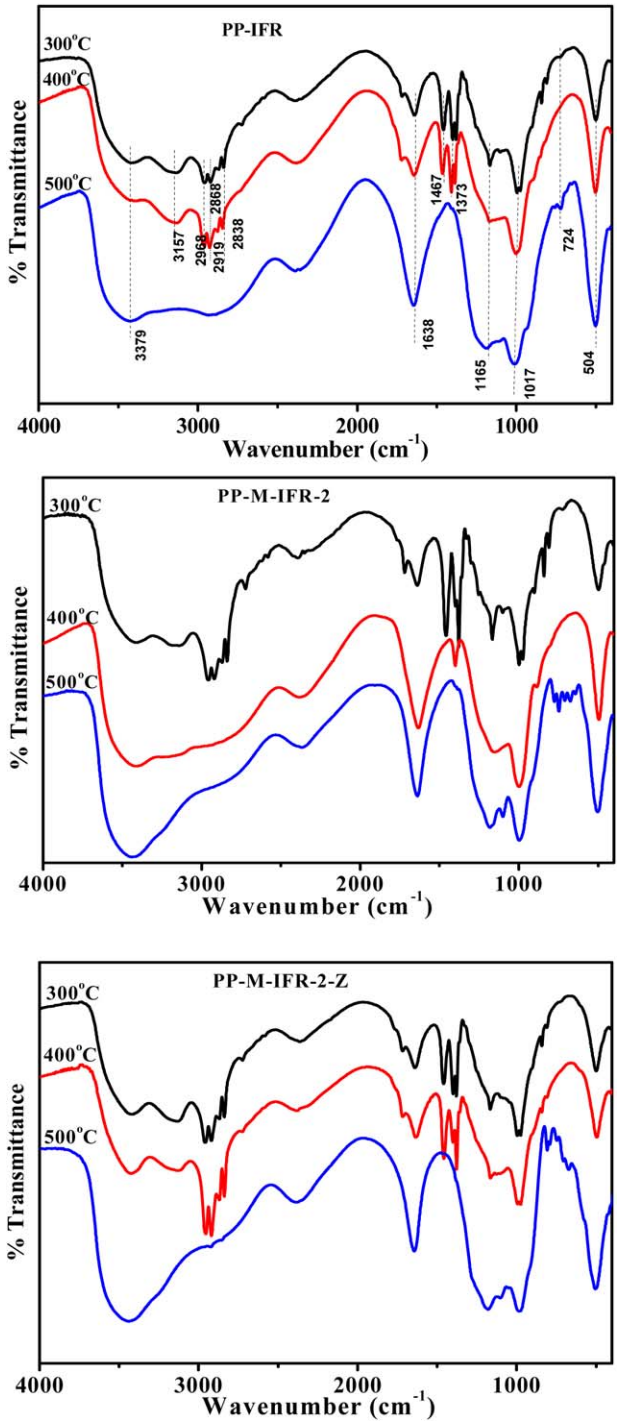

Figure 8. FTIR spectra of the PP-IFR, PP-M-IFR-2, and PP-M-IFR-2–Z char. [Color figure can be viewed in the online issue, which is available at wileyonlinelibrary.com.]

probably due to the lower heat stability of MAP. In the presence of Z, this phenomenon did not occur; this indicated that the carbonation promoted by Z was favorable for the stability of C—H bonds under the char layer. The scheme of the chemical reactions during the decomposition of PP-IFR is shown as follows:

Table VI. Mechanical Properties of the PP-IFR composites

Sample	Tensile strength (MPa)	Flexural strength (MPa)	Impact strength (kJ/m^2)
PP	32	45	59
PP-MAP	31	47	43
PP-IFR	25	41	18
PP-M-IFR-1	26	45	20
PP-M-IFR-2	27	46	22
PP-M-IFR-1-Z	32	49	20
PP-M-IFR-2-Z	33	52	20
PP-M-IFR-1-Z-CNT	33	53	25
PP-M-IFR-2-Z-CNT	33	55	26

1. Esterification reaction

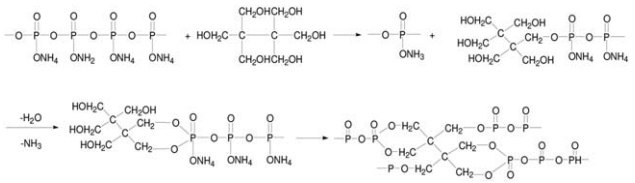

2. Thermal cracking and crosslinking into carbon

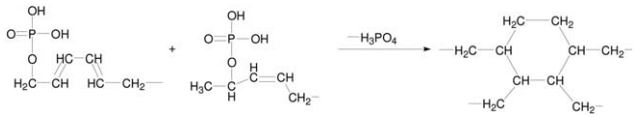

Mechanical Properties

The effects of additives on the mechanical properties of the composites were investigated. As shown in Table VI, the tensile, flexural, and impact strengths of the pure PP were 32 MPa, 45 MPa, and 59 kJ/m^2, respectively. With the presence of APP-s and DPER, significant decreases in the mechanical properties were observed, especially for the impact strength, which decreased by 70% because of the poor compatibility between the hydrophobic PP matrix and the hydrophilic flame retardants. With the incorporation of MAP into PP-IFR, the tensile and flexural strengths increased to some extent; this was probably due to the increase in the compatibility between the additives and the PP matrix. It was interesting to find that the tensile and flexural strengths were greatly promoted by the addition of Z. The former increased from 27 to 33 MPa, and the latter increased from 46 to 53 MPa. Moreover, in a combination with 0.05 wt % CNT, the impact strength increased from 20 to 25 kJ/m^2, whereas the tensile and flexural strengths increased slightly. The increase in CNT loading to 0.1 wt % did not significantly improve the impact strength. Compared with PP, the impact strength of PP-M-IFR-2–Z–CNT was still low. Here, CNTs could not overcome stress concentration; this completely resulted from IFR, and we indeed need to explore further effective methods.

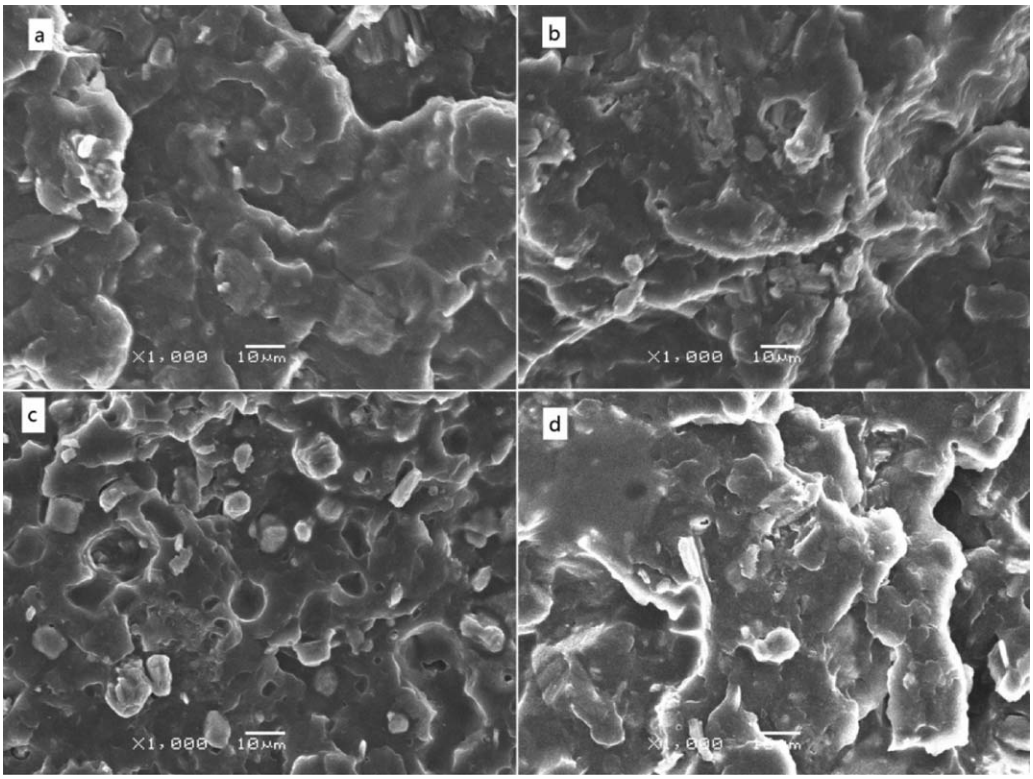

Figure 9. SEM micrographs of the composites: (a) PP-IFR, (b) PP-M-IFR-2, (c) PP-IFR-2–Z, and (d) PP-M-IFR-2–Z.

Morphologies of the Composites

The fractures of the PP-IFR composites obtained through impacting were observed by SEM (Figure 9). The PP-IFR sample presented the PP continuous phase with an obvious dispersion of IFR islands [Figure 9(a)], whereas the IFR islands on PP-M-IFR-2 decreased to a significant extent [Figure 9(b)]. the On PP-IFR–Z composite containing APP-r, there were many holes with sizes of less than 10 μm [Figure 9(c)]; this was due to the separation of Z from the PP matrix and indicated that the interfacial interaction between Z and PP was poor. These holes disappeared with the addition of MAP [Figure 9(d)]. Moreover, the fracture surface became more rough; this indicated that the compatibility was promoted significantly, probably because MAP could combine nonpolar PP with polar IFR and Z through nonpolar main chains and strong-polarity side groups. As a result, the mechanical properties of the composites were improved.

CONCLUSIONS

The solvation test showed that the solubility in water of APP-s obtained with MHS treatment was much lower than that of APP-r. The PP-IFR composites prepared by the incorporation of APP-s, DPER, MAP, Z, and CNTs in a twin-screw extruder presented good mechanical properties and thermal stability. With an APP-s/DPER ratio of 2:1, the LOI values of the PP-IFR composites were in the range 32.5–35.6%. The high flame retardancy of the PP-IFR composites was related to the greater number of char residues. The addition of MAP significantly improved the interaction between the PP matrix and additives. For PP-IFR, PP-M-IFR-2, and P-M-IFR-2–Z, the peak HRR values decreased from 930 to 347, 380, and 209 kW/m^2. THR decreased in the order PP-M-IFR-2 < PP-IFR < P-M-IFR-2–Z. The addition of 0.1% CNTs increased the impact strength of the PP-IFR composites from 18 to 26 kJ/m^2, and the flexural strength and tensile strength increased to 55 and 33 MPa, respectively.

ACKNOWLEDGMENTS

This research was supported by the Development Program for the National Natural Science Foundation of China (contract grant numbers 21277047 and 21307033).

REFERENCES

1. Zhang, S. Q.; Li, B.; Lin, M.; Li, Q. F.; Gao, S. L.; Yi, W. *J. Appl. Polym. Sci.* **2011**, *122*, 3430.
2. Feng, C. M.; Zhang, Y.; Liu, S. W.; Chi, Z. G.; Xu, J. R. *J. Appl. Polym. Sci.* **2012**, *123*, 3208.
3. Deng, C. L.; Du, S. L.; Zhao, J.; Shen, Z. Q.; Deng, C.; Wang, Y. Z. *Polym. Degrad. Stab.* **2014**, *108*, 97.
4. Yi, J. S.; Liu, Y.; Pan, D. D.; Cai, X. F. *J. Appl. Polym. Sci.* **2013**, *127*, 1061.
5. Jian, R. K.; Li, C.; Chen, S. Y.; Long, J. W.; Wang, Y. Z. *Polym. Degrad. Stab.* **2014**, *109*, 184.
6. Zhang, R.; Huang, H.; Yang, W.; Xiao, X. F.; Hu, Y. *J. Appl. Polym. Sci.* **2012**, *125*, 3946.
7. Mohammad, M. A.; Majid, A.; Gity, M. S. *J. Appl. Polym. Sci.* **2013**, *127*, 1683.

8. Shao, Z. B.; Deng, C.; Tan, Y.; Chen, M. J.; Li, C. *Polym. Degrad. Stab.* **2014**, *106*, 88.
9. Wu, K.; Song, L.; Wang, Z. Z.; Hu, Y. *J. Polym. Res.* **2009**, *16*, 283.
10. Qian, L. J.; Feng, F. F.; Tang, S. *Polymer* **2014**, *55*, 95.
11. Ullah, S.; Ahmad, F. *Polym. Degrad. Stab.* **2014**, *103*, 49.
12. Ma, Z. L.; Fan, C. R.; Lu, G. Y.; Liu, X. Y.; Zhang, H. *J. Appl. Polym. Sci.* **2012**, *125*, 3567.
13. Yang, D. D.; Hu, Y.; Song, L.; Nie, S. B.; He, S. Q.; Cai, Y. B. *Polym. Degrad. Stab.* **2008**, *93*, 2014.
14. Yang, L.; Cheng, W. L.; Zhou, J.; Li, H. L.; Wang, X. L.; Chen, X. D.; Zhang, Z. Y. *Polym. Degrad. Stab.* **2014**, *105*, 150.
15. Zhang, J. J.; Ji, Q.; Wang, F. J.; Tan, L. W.; Xia, Y. Z. *Polym. Degrad. Stab.* **2012**, *97*, 1034.
16. Feng, C. M.; Zhang, Y.; Liu, S. W.; Chi, Z. G.; Xu, J. R. *Polym. Degrad. Stab.* **2012**, *97*, 707.
17. Seongchan, P.; Takashi, K.; Daniel, S.; Jaseung, K.; Si, M. Y.; Jonathan, C. S.; Rafailovich, M. H. *Macromolecules* **2009**, *42*, 6698.
18. Demir, H.; Arkısx, E.; Balkose, D.; Ulku, S. *Polym. Degrad. Stab.* **2005**, *89*, 478.
19. Rousseaux, D. D. J.; Naïma, S. I.; Baudouin, B.; Devaux, A. C.; Godard, J.; Jacqueline, P. *Polymer* **2011**, *52*, 443.
20. Tiwari, R. R.; Paul, D. R. *Polymer* **2011**, *52*, 5595.
21. Spencer, M. W.; Hunter, D. L.; Knesek, B. W.; Paul, D. R. *Polymer* **2011**, *52*, 5369.
22. Jia, Y. Y.; Chen, Z. R.; Yan, W. Y. *Compos. Sci. Technol.* **2014**, *91*, 38.
23. Wu, Z. F.; Xue, M.; Wang, H.; Tian, X. Y.; Cu, P. *Polymer* **2013**, *54*, 3334.
24. Huang, Y. W.; Song, M. L.; Ma, J. J.; Lu, Z. Y.; Yang, J. X.; Cao, K. *J. Appl. Polym. Sci.* **2013**, *129*, 316.
25. Vennerberg, D.; Rueger, Z.; Kessler, M. R. *Polymer* **2014**, *55*, 1854.
26. Rahmanian, S.; Suraya, A. R.; Shazed, M. A.; Zahari, R.; Zainudin, E. S. *Mater. Des.* **2014**, *60*, 34.
27. Ren, F.; Zhang, X. J.; Wei, Z.; Chen, J. F.; Dong, D. W.; Li, X. L.; Zhang, L. Q. *J. Appl. Polym. Sci.* **2013**, *129*, 2261.
28. Deng, C.; Zhao, J.; Deng, C. L.; Lv, Q.; Chen, L.; Wan, Y. Z. *Polym. Degrad. Stab.* **2014**, *103*, 1.
29. Walid, H. A.; Charles, A. W. *Polymer* **2010**, *51*, 2277.
30. Shang, Y. Y.; Li, Y. B.; He, X. D.; Du, S. Y.; Zhang, L. H.; Shi, E. Z.; Wu, S. T.; Li, Z.; Li, P. X.; Wei, J. Q.; Wang, K. L.; Zhu, H. W.; Wu, D. H.; Cao, A. Y. *ACS Nano* **2013**, *7*, 1446.